Supporting Information

Adjusting interfacial chemistry and electronic properties of photovoltaics based on a highly pure Sb_2S_3 absorber by atomic layer deposition

Pascal Büttner,[†] Florian Scheler,[†] Craig Pointer,[‡] Dirk Döhler,[†] Maïssa K. S. Barr,[†] Aleksandra Koroleva,[¶] Dmitrii Pankin,[§] Ruriko Hatada,[‖] Stefan Flege,[‖] Alina Manshina,[⊥] Elizabeth R. Young,[*,‡] Ignacio Mínguez-Bacho,[*,†] and Julien Bachmann[*,†,⊥]

†*Chemistry of Thin Film Materials, Department of Chemistry and Pharmacy, Friedrich-Alexander University Erlangen-Nürnberg, Cauerstr. 3, Erlangen, 91058 Germany*

‡*Department of Chemistry, Lehigh University, 6 E. Packer Ave., Bethlehem, PA 18015 USA*

¶*Centre for Physical Methods of Surface Investigation, St. Petersburg State University, St. Petersburg, 198504 Russia*

§*Centre for Optical and Laser Materials Research, St. Petersburg State University, St. Petersburg, 199034 Russia*

‖*Materials Analysis, Department of Materials Science, Technische Universität Darmstadt, Alarich-Weiss-Str. 2, Darmstadt, 64287 Germany*

⊥*Institute of Chemistry, Saint-Petersburg State University, Universitetskii pr. 26, St. Petersburg, 198504 Russia*

E-mail: ery317@lehigh.edu; ignacio.minguez@fau.de; julien.bachmann@fau.de

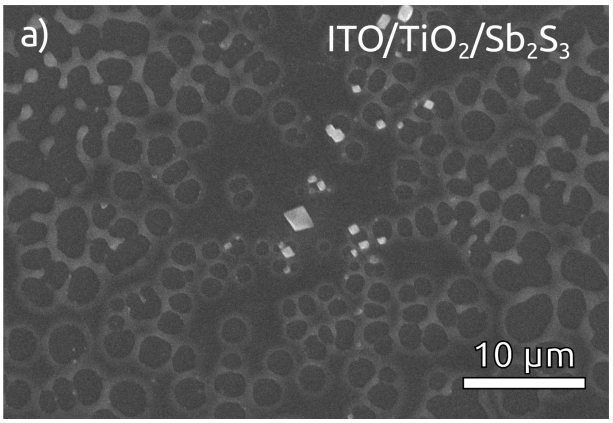

Figure S1: Dewetting of Sb_2S_3 on ITO / TiO_2 without ZnS.

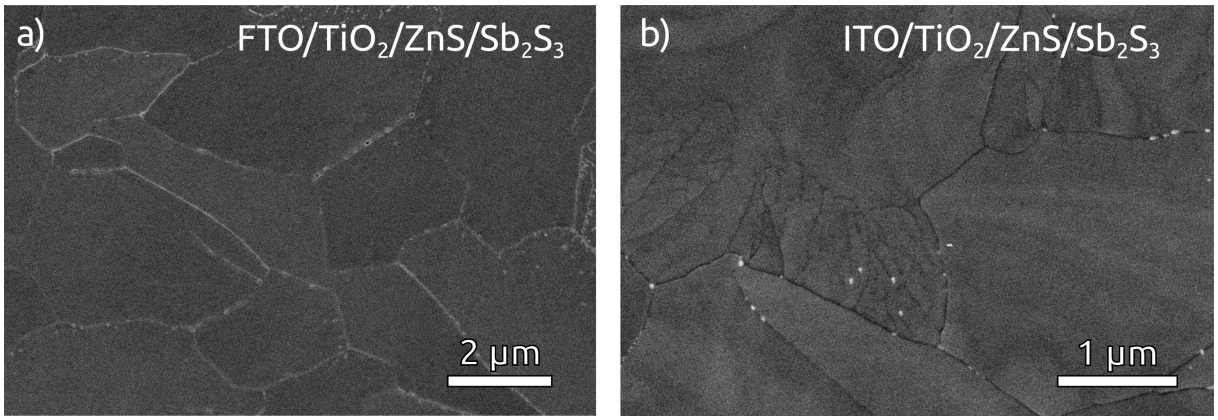

Figure S2: Sb_2S_3 grains formed upon annealing with 1.5 nm ZnS on a) FTO / TiO_2. and b) sputtered ITO / TiO_2.

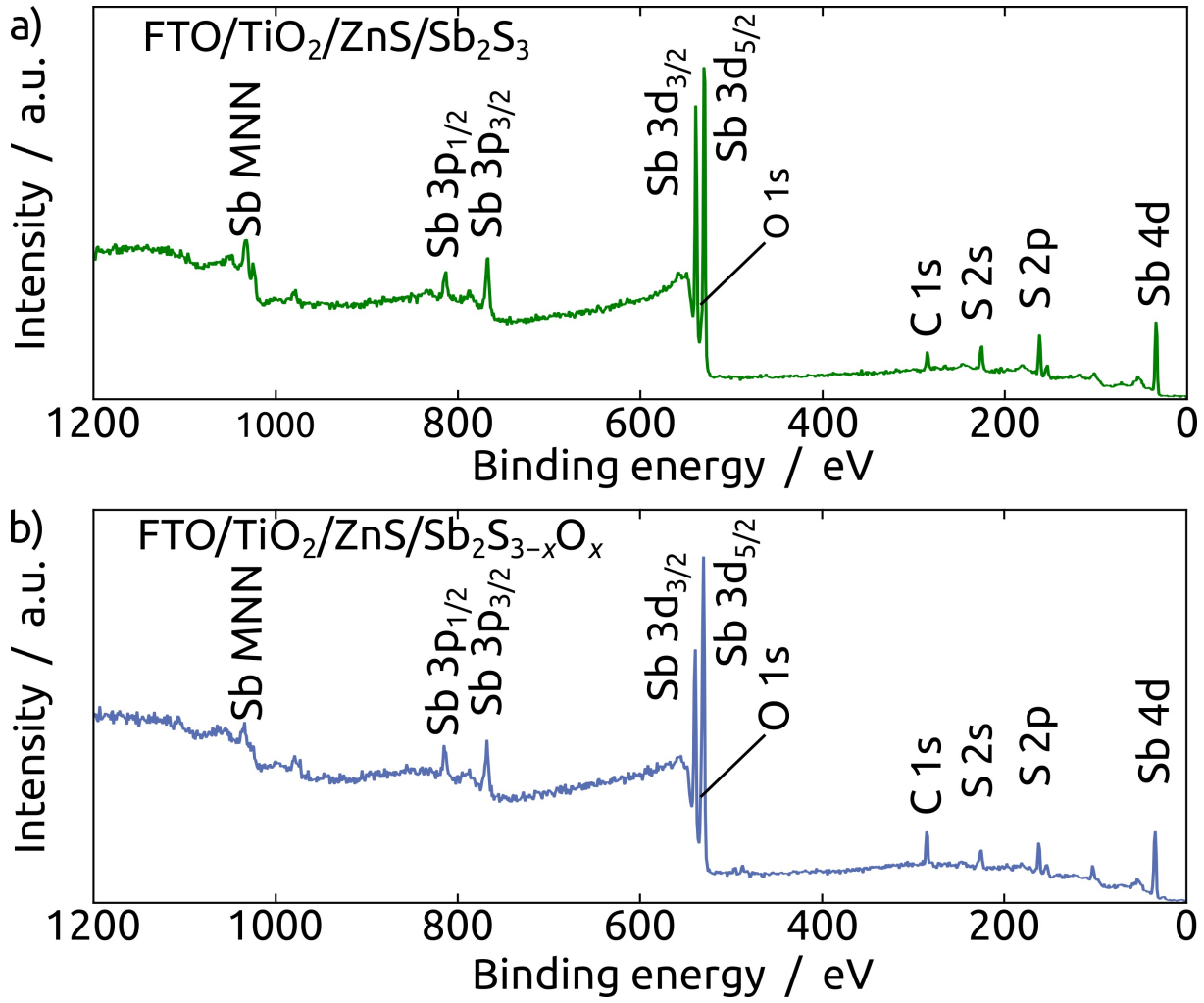

Figure S3: XPS surveys for a) highly pure Sb_2S_3 and b) oxygen containing $Sb_2S_{3-x}O_x$. The O 1s signal overlaps with the Sb $3d_{5/2}$ signal.

Table S1: Raman band center positions observed experimentally and assignments with symmetry and phonon mode descriptions as stated in the corresponding references. Literature references are for the pure, crystalline phases Sb_2S_3 (stibnite) and Sb_2O_3 (kermesite).

Observed wavenumber [cm^{-1}]	Assignment	Wavenumber from literature [cm^{-1}]
	Antimony sulfide	
156	A_g (lattice mode)	155;[1] 158[2]
191	B_{1g} (antisymmetric bending)	189;[1] 186;[2] 190;[3] 192;[4] 188[5]
207	B_{1g} (antisymmetric bending)	207[3,4]
238	B_{1g} (symmetric bending)	237;[1,3,5] 239[2,4]
282	A_g (antisymmetric stretching)	281;[1,5] 282;[2,3] 283[4]
301	B_{1g} (antisymmetric stretching)	299;[2] 300;[1,3] 301;[5] 303[4]
313	B_{1g} (symmetric bending)	306;[3] 310;[1,4,5] 312[2]
	Antimony oxide	
246	B_{1g} (antisymmetric bending)	245[1]
288	B_{1g} (symmetric bending)	289[1]
305	A_g (antisymmetric stretching)	303[1]
317	B_{1g} (antisymmetric stretching)	317[1]

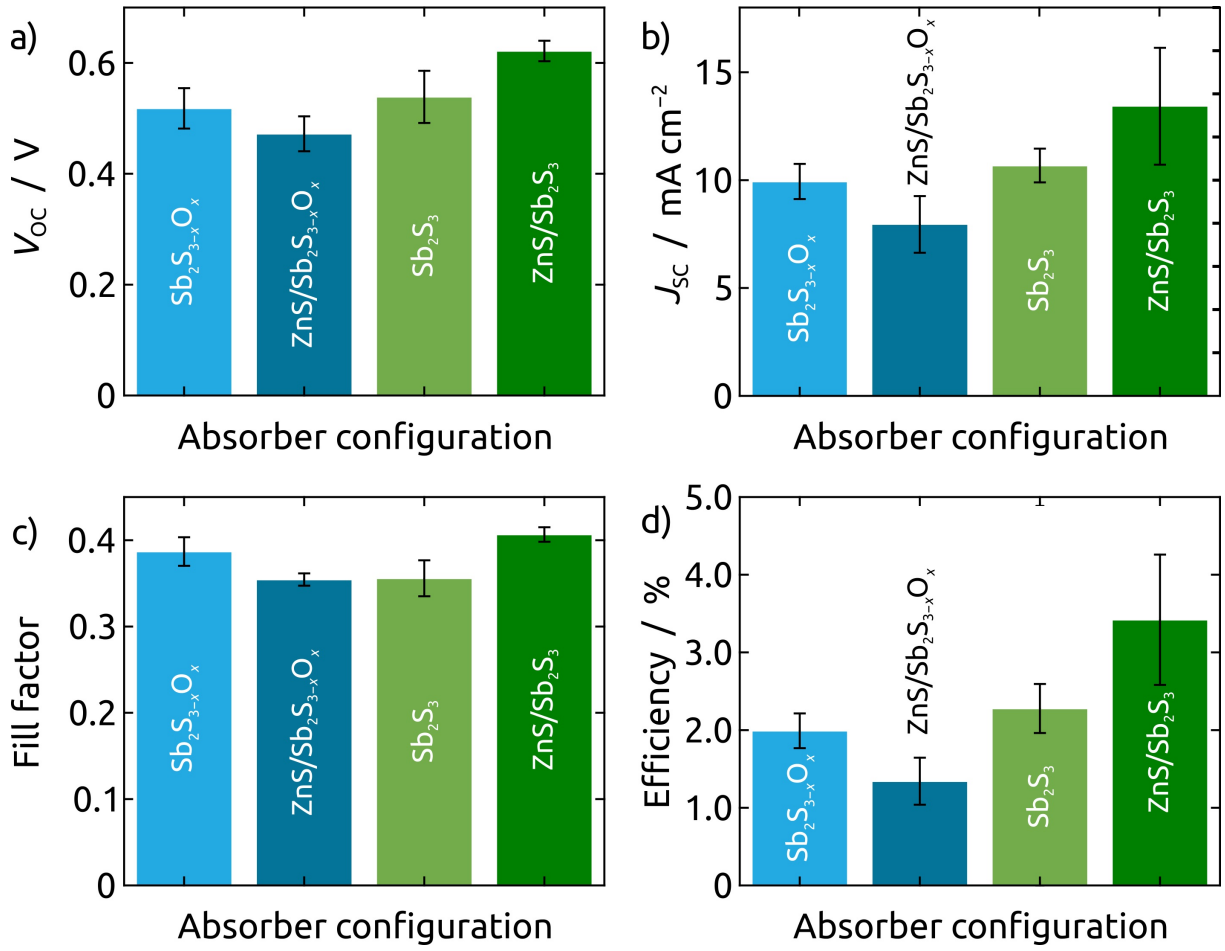

Figure S4: Photovoltaic parameters a) V_{oc}, b) J_{sc}, c) FF and d) Power conversion efficiency of the solar cell devices with $Sb_2S_{3-x}O_x$, ZnS / $Sb_2S_{3-x}O_x$, Sb_2S_3 and ZnS / Sb_2S_3.

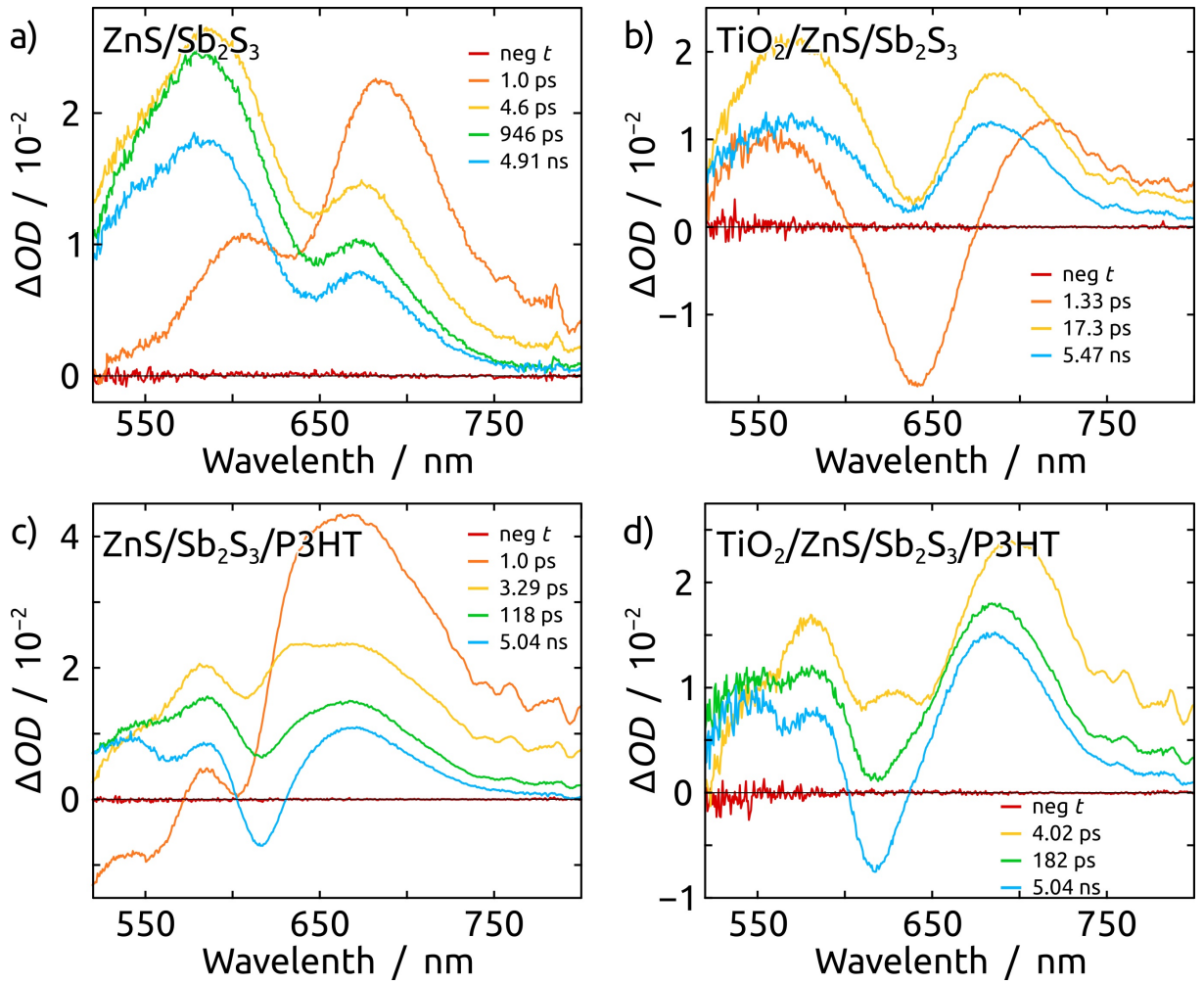

Figure S5: Transient absorption spectra recorded at negative time and four distinct positive times for each of the four semiconductor stack configurations. a) Configuration **A**, ZnS/Sb_2S_3, b) Configuration **B**, $TiO_2/ZnS/Sb_2S_3$, c) Configuration **C**,ZnS/Sb_2S_3/P3HT, c) Configuration **D**, $TiO_2/ZnS/Sb_2S_3$.

Table S2: Summary of lifetimes (and associated uncertainties) obtained for each DADS of each configuration.

Sample	Structure	τ_1 [ps]	τ_2 [ns]	τ_3 [ns]
A	ZnS / Sb_2S_3	1.69 (0.02)	-	10.3 (0.2)
B	TiO_2 / ZnS / Sb_2S_3	2.6 (0.2)	4.9 (0.8)	14 (2)
C	ZnS / Sb_2S_3 / P3HT	1.1 (0.2)	0.3 (0.1)	10 (2)
D	TiO_2 / ZnS / Sb_2S_3 / P3HT	2.2 (0.2)	0.41 (0.08)	13 (2)

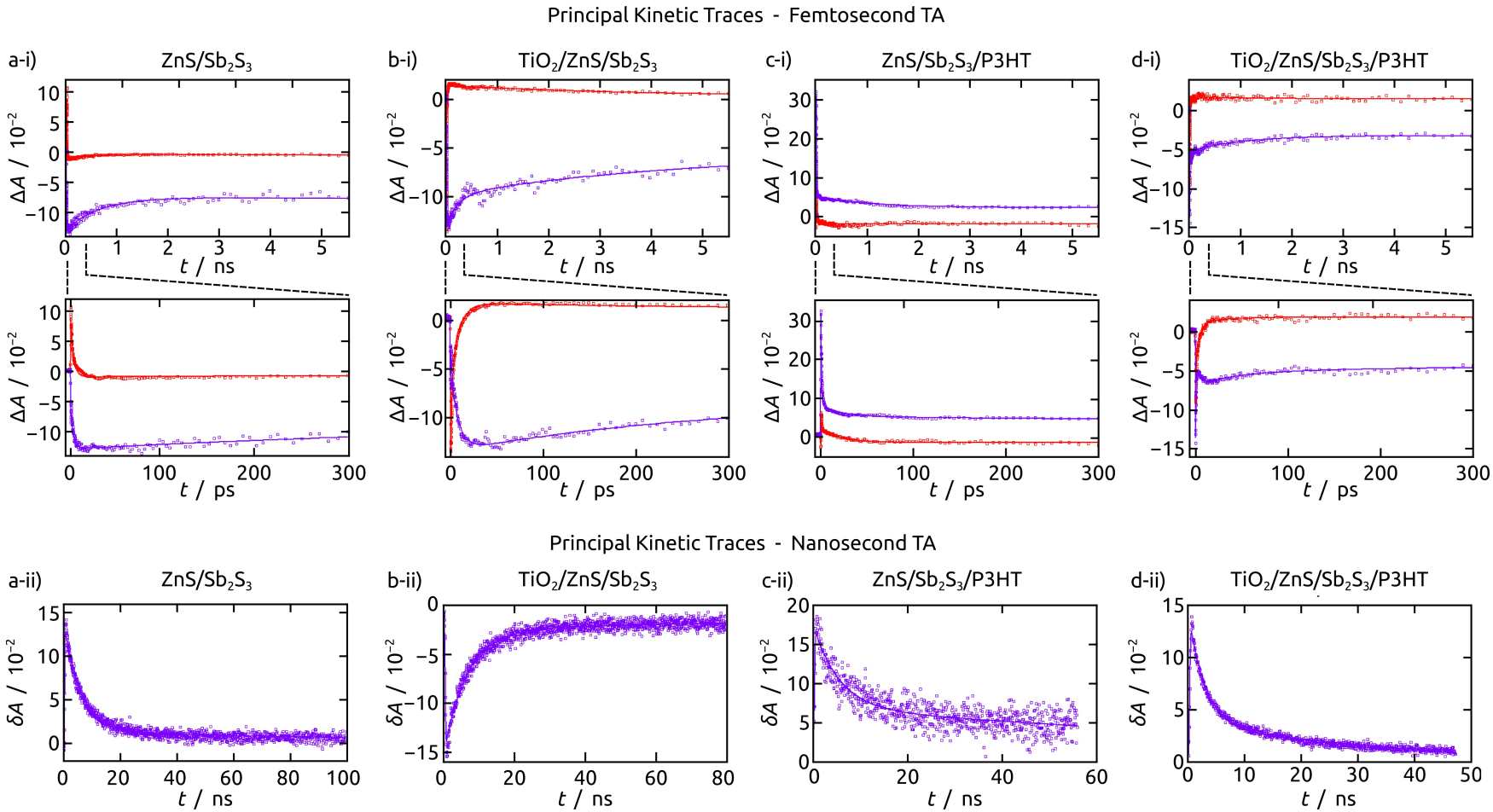

Figure S6: Results of the global analysis fitting for a) ZnS/Sb_2S_3, b) $TiO_2/ZnS/Sb_2S_3$, c) ZnS/Sb_2S_3/P3HT, and d) $TiO_2/ZnS/Sb_2S_3$/P3HT samples from Figure 6 with the principal kinetic traces for each data set. The solid lines of the principal kinetics traces represent the multiexponential fit to the data, which are shown as the dotted lines, for both the (i) femtosecond transient absorption (TA) data (1^{st} and 2^{nd} rows) and (ii) nanosecond TA data (3^{rd} row). The red and purple lines represent the 1st and 2nd principal components from the femtosecond dataset. Femtosecond principal kinetic traces are shown for the entire 5-ns window (2^{nd} row) as well zoomed in for the first 300 ps (2^{nd} row) to show that the fit captures the entire temporal range. The nanosecond TA data shows only one principal component that is shown in purple.

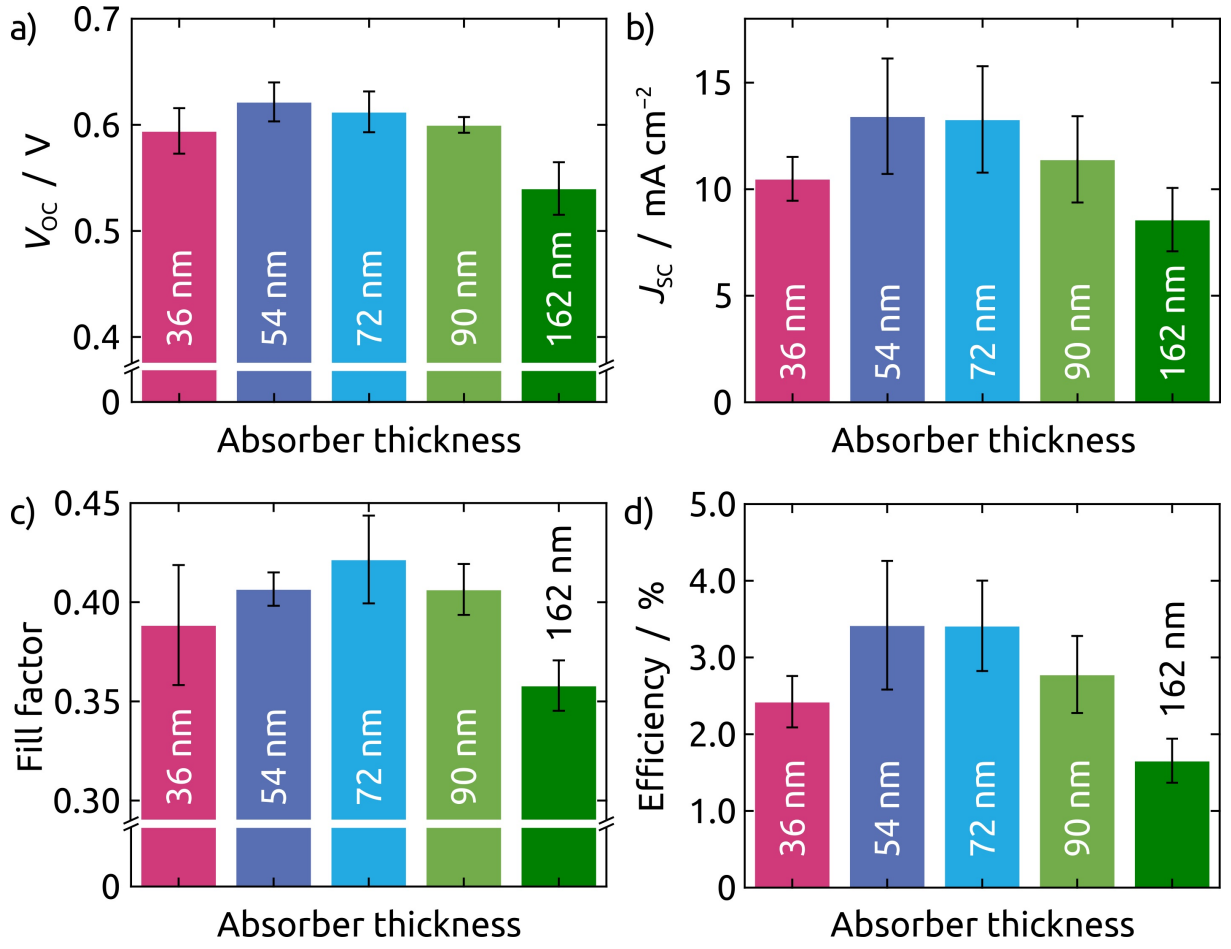

Figure S7: Photovoltaic parameters of solar cell devices with Sb_2S_3 thicknesses of 36, 54, 72, 90 and 162 nm: a) V_{oc}, b) J_{sc}, c) *FF* and d) Power conversion efficiency. The bars represent average values and the error bars the standard deviation.

References

(1) Kharbish, S.; Libowitzky, E.; Beran, A. Raman spectra of isolated and interconnected pyramidal XS_3 groups (X = Sb,Bi) in stibnite, bismuthinite, kermesite, stephanite and bournonite. *Eur. J. Mineral.* **2009**, *21*, 325–333.

(2) Ibanez, J.; Sans, J. A.; Popescu, C.; Lopez-Vidrier, J.; Elvira-Betanzos, J. J.; Cuenca-Gotor, V. P.; Gomis, O.; Manjon, F. J.; Rodriguez-Hernandez, P.; Munoz, A. Structural, Vibrational, and Electronic Study of Sb_2S_3 at High Pressure. *J. Phys. Chem. C* **2016**, *120*, 10547–10558.

(3) Kharbish, S. Raman spectroscopic investigations of some Tl-sulfosalt minerals containing pyramidal (As,Sb)S_3 groups. *Am. Mineral.* **2011**, *96*, 609–616.

(4) Sereni, P.; Musso, M.; Knoll, P.; Blaha, P.; Schwarz, K.; Schmidt, G. Polarization-Dependent Raman Characterization of Stibnite (Sb_2S_3). *AIP Conf. Proc.* **2010**, *1267*, 1131–1132.

(5) Eensalu, J. S.; Katerski, A.; Karber, E.; Acik, I. O.; Mere, A.; Krunks, M. Uniform Sb_2S_3 optical coatings by chemical spray method. *Beilstein J. Nanotech.* **2019**, *10*, 198–210.